Evidence of Surface Properties by Isopropanol Decomposition Reaction and NH3-TPD over Ni–Fe Spinel Nanoparticles Prepared via Hydrothermal Route

Rafik Benrabaa, Annick Rubbens, Axel Löfberg, Rose-Noelle Vannier

ChemistrySelect

Research Article
doi.org/10.1002/slct.202204361

Chemistry Europe
European Chemical Societies Publishing

www.chemistryselect.org

Evidence of Surface Properties by Isopropanol Decomposition Reaction and NH_3-TPD over Ni–Fe Spinel Nanoparticles Prepared *via* Hydrothermal Route

Rafik Benrabaa,*[a, b] Annick Rubbens,[c] Axel Löfberg,*[c] and Rose-Noëlle Vannier[c]

In this work, surface properties evaluated by catalytic conversion of isopropanol and by ammonia Temperature Programmed Reduction (NH_3-TPD) over ferrite spinel nanoparticles was investigated. Bulk $NiFe_2O_4$ with specific surface area 114 m^2/g and crystallites size 6 nm was prepared by hydrothermal synthesis using nitrates as precursors. X-ray diffraction (XRD), Raman spectroscopy, specific surface area by B.E.T, Scanning Electron Microscopy (SEM) and X-ray energy dispersive microanalysis (EDS), Transmission Electron Microscopy (TEM) and X-ray Photoelectron Spectroscopy (XPS) techniques were used for their structural and textural characterizations. The reducibility by hydrogen at variable temperatures was investigated by Temperature Programmed reduction (H_2-TPR) and Thermal Gravimetric Analysis- Differential Scanning Calorimetry (TGA-DSC). The total acidity and acid strength distribution was determined by NH_3-TPD. The synthesized oxide showed the presence of mixed phases containing the inverse spinel structure $NiFe_2O_4$ as the major phase and iron oxide α-Fe_2O_3 as an additional phase. It was shown that the surface of the powder was richer in Ni^{2+} species. The surface acidity (Brönsted and Lewis) determined by NH_3-TPD showed that the number of acidic sites increased dramatically with the temperature. The catalytic conversion of isopropanol yields both acidic and redox/basic sites were available. A good correlation between textural, structural, redox and acid-base properties of catalyst is established.

Introduction

The study of the acidity of bulk oxides is of great importance for applications of these materials, particularly in the petrochemical industry and environmental sciences. In order to design materials with high activity and selectivity, a detailed characterization of the active sites is required. A question of basic interest is to determine the correlation between these properties and the promotion of catalytic activity of oxides.

Several methods have been successfully used to study the active sites. These methods are based on the adsorption/desorption of probe molecules. Among the methods commonly applied, temperature-programmed desorption (TPD)[1] or adsorption microcalorimetry[2–4] of probe molecules give information regarding the distribution and strength of active sites located on the surface. Spectroscopic methods, such as infrared (IR), nuclear magnetic resonance (NMR) or X-ray photoelectron spectroscopy (XPS) have also been extensively used to study the nature of acid-base properties.[5,6]

The adsorption of alcohols over oxide catalysts has been used as a chemical probe reaction for many years. Isopropanol decomposition reaction is one of the main methods for determining surface acid-base properties.[7,8] The decomposition leads to the formation of olefins, ether, ketones, carbon monoxide or dioxide. If the solid exhibits acidic properties, only the dehydration products (ether + olefins) are obtained, whereas if the catalyst displays basic or redox properties, dehydrogenation of the alcohol is observed (ketone formation).[9,10] Depending on the nature of the catalyst and the operating conditions chosen, one or the other of the reaction paths can be favoured.

The various reactions usually accepted to describe the decomposition of isopropanol can be summarized as follows:

Without oxygen:

$$2(CH_3)_2\text{-CH-OH} \rightarrow (CH_3)_2CH\text{–O-}CH(CH_3)_2 + H_2O : \quad (1)$$

deshydratation, diisopropylether

$$(CH_3)_2\text{-CH-OH} \rightarrow CH_3CH{=}CH_2 + H_2O : \quad (2)$$

deshydratation, propylene

$$(CH_3)_2\text{-CH-OH} \rightarrow CH_3\text{-CO-}CH_3 + H_2 : \quad (3)$$

deshydrogenation, acetone

With oxygen:

[a] *Prof. R. Benrabaa*
Laboratoire de Physico-Chimie des Matériaux, Faculté des Sciences et de la Technologie, Université Chadli BENDJEDID-El Tarf, B.P 73 El Tarf 36000, Algérie
E-mail: r.benrabaa@univ-eltarf.dz
[b] *Prof. R. Benrabaa*
Laboratoire de Matériaux Catalytiques et Catalyse en Chimie Organique, Faculté de Chimie, USTHB, BP32, El-Alia, 16111 Bab Ezzouar, Alger, Algérie
[c] *Prof. A. Rubbens, Dr. A. Löfberg, Prof. R.-N. Vannier*
Univ. Lille, CNRS, Centrale Lille, Univ. Artois, UMR 8181 – UCCS – Unité de Catalyse et Chimie du Solide, F-59000 Lille, France
E-mail: axel.lofberg@univ-lille.fr

$(CH_3)_2$-CH-OH + 1/2O_2 → CH_3-CO-CH_3 + H_2O : Oxy-deshydrogenation (4)

$(CH_3)_2$-CH-OH + 9/2O_2 → 3CO_2 + 4H_2O : total Combustion (5)

$(CH_3)_2$-CH-OH + 3O_2 → 3CO + 4H_2O : incomplete combustion (6)

The decomposition reaction of isopropanol can be carried out in the absence (reactions 1, 2 and 3) or in the presence of gaseous oxygen (reactions 4, 5 and 6). In the presence of oxygen, isopropanol can undergo an oxidation-hydrogenation reaction to form acetone (reaction 4) or a combustion reaction which leads to the formation of carbon dioxide or carbon monoxide (reactions 5 and 6) depending on whether the reaction mixture is poor or rich in oxygen.

It appears that the activities vary considerably from one solid to another. Selectivity is also very variable but in general, a solid having a basic character like MgO and CaO, exhibits a very low activity but a selectivity almost of 100% in acetone product. In contrast, an acidic solid such as V_2O_5 has high activity and selectivity for propylene of up to 94%.[11] The isopropanol decomposition is a method that does not allow to distinguish between the Brønsted and Lewis acidity. However, Aramendia *et al.*[12] have reported that the dehydration activity during isopropanol decomposition could be correlated with Brønsted acidity.

Spinels family are excellent materials in electronics for their ferromagnetic properties, in catalysis such as the reduction of NOx, the decomposition of alcohols and the reforming of hydrocarbons.[8,12–15] The catalytic activity of spinels depends essentially on (i) the degree of substitution of the cations and the degree of inversion of the spinel structure, (ii) the preparation method and departure precursors, (iii) the presence of a support and (iv) the distribution of species on the catalytic surface. These parameters considerably influence the acid-base behavior of the catalysts and consequently its catalytic activity. Indeed, the study of the acidity of the catalysts is a key point for understanding the mechanism of the catalytic act.

A previous work in dry reforming of methane,[16] we showed that the activity of nickel ferrite could be correlated to the surface acidity that would limit the relative contribution of Reverse Water Gas Shift reaction. For a better insight of the acidity of catalyst prepared via hydrothermal synthesis, it was reinvestigated. In this work, $NiFe_2O_4$ spinel oxide issued from hydrothermal method was prepared under other conditions compared to our previous. The structural, textural and surface composition as well as redox properties was studied in details and then correlated to the catalytic conversion of isopropanol.

Results and discussion

Structural (XRD and Raman), surface (BET, XPS, SEM and TEM) and bulk composition (EDS)

The phase composition, purity and structure of the products were ascertained by XRD and Raman analysis at room temperature. Figure 1 displays the XRD patterns of $NiFe_2O_4$ spinel oxide. The registered diffractogram shows only the lines characteristic of pure $NiFe_2O_4$ (*PDF 00-054-0954*) structure with the main peaks at $2\theta° \approx 18.4$ w (*111*), 30.4 m (*220*), 35.7 vs (*311*), 37.3 w (*222*), 43.4 m (*400*), 53.9 w (*422*), 57.3 m (*511*) and 62.9 m (*440*). (intensity of lines, w: weak, m: medium, s: strong; vs: very strong; *hkl* in brackets) (Figure 1, left). No lines corresponding to nickel or iron free oxides, could be observed.

The XRD pattern of $NiFe_2O_4$ spinel oxide was refined using Rietveld method. The structural model corresponding to $NiFe_2O_4$ spinel (Fd-3 m)[17] was introduced in the refinement. The refinement led to a = 8.377(5) Å and crystallite size Cs = 6 nm.

The bulk ferrite powder was further investigated using laser Raman spectroscopy in order to ascertain the structure of the catalyst. The Raman spectrum is given in Figure 1 (right). The Raman spectra of $NiFe_2O_4$ spinel oxide show the characteristic vibrational modes of the $NiFe_2O_4$ inverse spinel[18–20] There are located at wavenumbers: 702 cm^{-1} (s), 665 cm^{-1} (s), 579 cm^{-1}

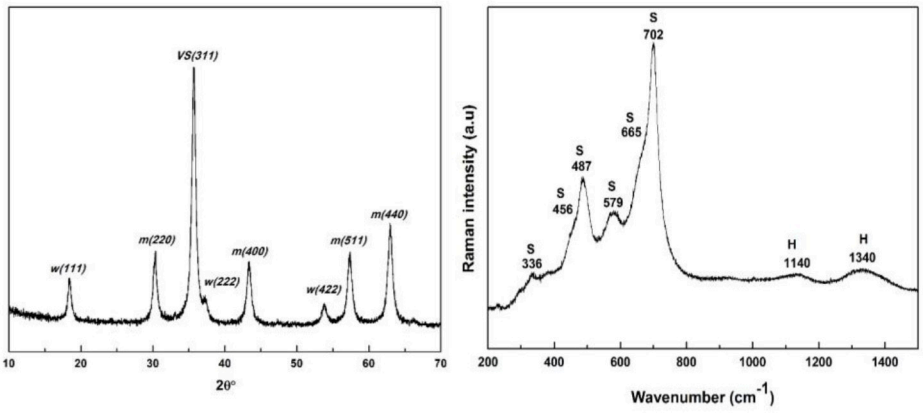

Figure 1. Structural properties by XRD (left) and Raman (right) of $NiFe_2O_4$ prepared via hydrothermal route at 180 °C/1 h.

(m, broad), 487 cm^{-1} (m), 456 cm^{-1} (s), 336 cm^{-1} (w). In contrast to XRD results which showed no peak corresponding to free oxides, two bands with low intensity at ~1140 cm^{-1} and 1340 cm^{-1} were observed and attributed to α-Fe_2O_3 hematite.[21,22]

The specific surface area of the catalyst was determined from the nitrogen adsorption-desorption isotherms at 77 K. $NiFe_2O_4$ sample treated at 180 °C for 1 hours under hydrothermal conditions showed a value of 114 m^2/g (Table 1). The N_2 adsorption-desorption isotherm of the catalyst (Figure 2-a), is type IV according to IUPAC classification with H3-type hysteresis loop, indicating mesoporous materials. The porosity of the catalyst was studied by the B.J.H method (Barrer, Joyner and Halenda) from the N_2 desorption isotherm assuming that the pores are cylindrical and open at both ends (Figure 2-b). the obtained results confirmed that $NiFe_2O_4$ prepared by HT technique at 180 °C/1 h is in mesoporous category (25–500 Å). SEM micrograph (Figure 3-left) confirmed monodisperse and highly nanoparticles distribution with small grain size. However, TEM image (Figure 3-right) showed ununiform nanosized particles with diffraction fringes were observed confirming that the high crystallinity of the sample as evidenced by the XRD pattern. The heterogeneity of $NiFe_2O_4$ powder suggested that the presence of a mixed phase in accordance with Raman spectroscopy showing the presence of $NiFe_2O_4$ and α-Fe_2O_3 hematite as supplementary phase. The crystal size measured in TEM image of the sample is smaller-around 10 nm. The elemental composition of $NiFeO_4$ sample was performed by EDS analysis. The measured Fe:Ni atomic ratio (~1.9) of analyzed sample was very similar to the nominal atomic ratio (Fe:Ni = 2) used in the hydrothermal preparation. The surface composition of catalyst was determined by XPS at room temperature. The Figure 4 represent the photoemission spectra of 2p levels of nickel (Ni2p3/2 line) and iron (Fe2p3/2 line). The presence of Ni^{2+} and Fe^{3+} was detected by Ni*2p3/2* (854.9 eV) and Fe*2p3/2* (710.7 eV) photopeaks, respectively.[23,24] The binding energies values obtained and the recorded shape (Figure 4)

Table 1. Crystallographic parameters, specific surface area and Ni/Fe ratio of $NiFe_2O_4$ catalyst.

	Cs[a] (nm)	a[b] (Å)	$S_{B.E.T}$[c] (m^2/g)	Ni/Fe[d]	Ni/Fe[e]
$NiFe_2O_4$	6	8.377(5)	114	1.9	1.9

[a] Crystallite size, [b] Lattice parameter, [c] Specific Surface Area, [d] Obtained by EDX, [e] Obtained by XPS

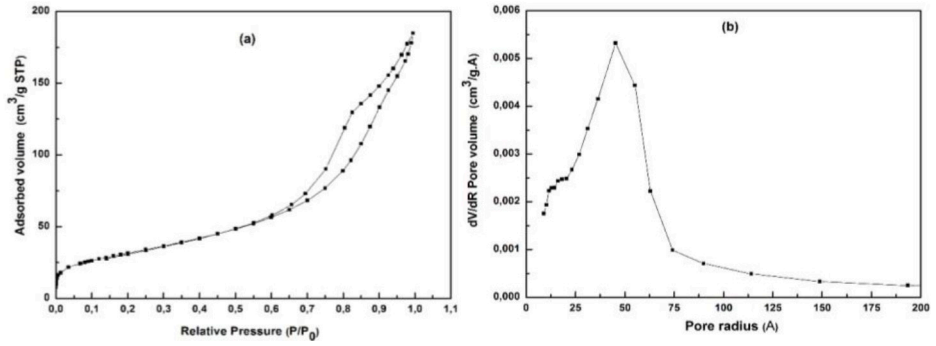

Figure 2. N_2 adsorption-desorption isotherm (a) and porous distribution of $NiFe_2O_4$ solid prepared via hydrothermal synthesis at 180 °C/1 h.

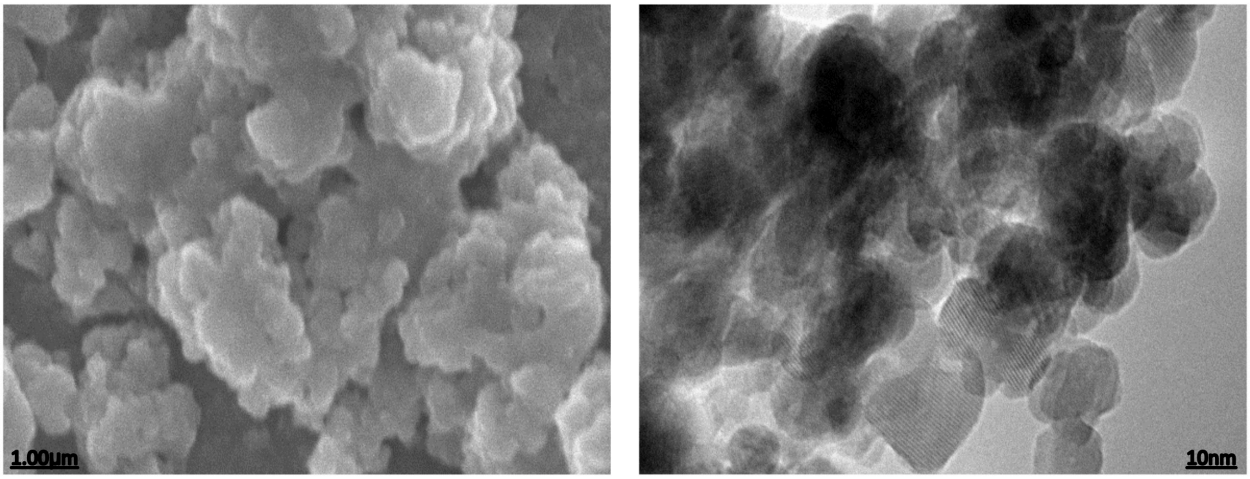

Figure 3. SEM (left) and TEM (right) micrographs of $NiFe_2O_4$ prepared via hydrothermal route at 180 °C/1 h.

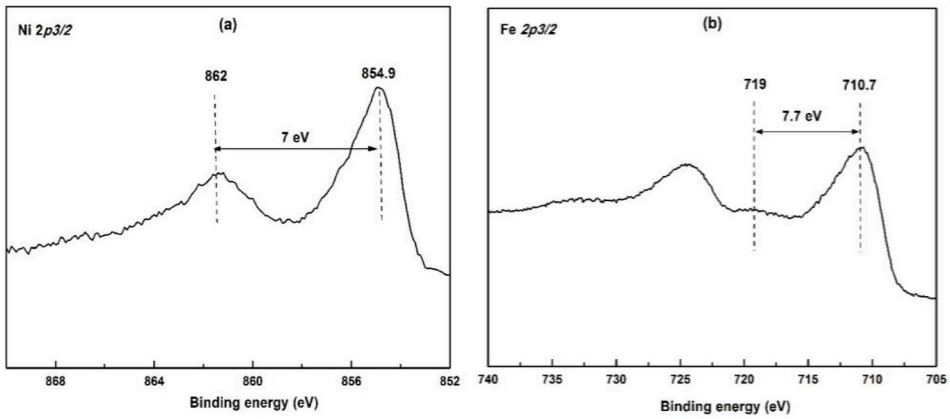

Figure 4. XPS spectra of Ni $2p_{3/2}$ (a) and Fe 2p3/2 (b) for $NiFe_2O_4$ solid prepared via hydrothermal synthesis at 180 °C/1 h.

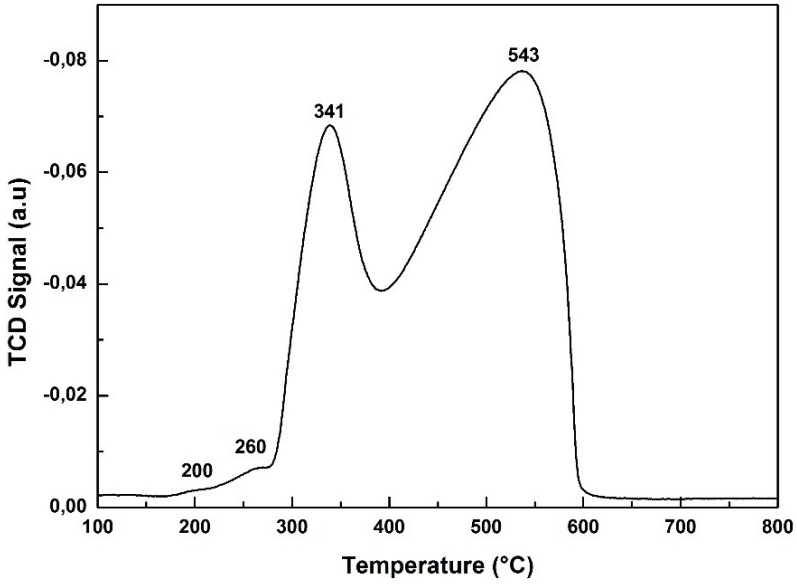

Figure 5. H_2-TPR profiles of bulk $NiFe_2O_4$ spinel oxide prepared by hydrothermal synthesis at 180 °C/1 h.

of the spectra for Ni and Fe cations confirm that both species are in $NiFe_2O_4$ spinel structure and in (II+) et (III+) oxidation state, respectively. The Fe:Ni surface ratio (~1.9) was very close to the expected value (Fe:Ni = 2) and in good agreement with Ni:Fe obtained by EDX experiments (Table 1). EDS and XPS results are not in the same trend of Raman spectroscopy which confirming a mixed phase in the $NiFe_2O_4$ structure. We were waiting an atomic ratio Fe:Ni > 2 (bulk and surface richer in Fe species) for justify the presence of α-Fe_2O_3 observed by Raman analysis. These results suggest that, in our hydrothermal synthesis conditions, a very low amount of α-Fe_2O_3 hematite was formed beside $NiFe_2O_4$ structure.

Reducibility study (H_2-TPR and H_2-TGA-DSC)

The reduction behavior of bulk $NiFe_2O_4$ spinel oxide prepared by hydrothermal method was followed by H_2-TPR and TGA-DSC at variable temperature under H_2 atmosphere. The amount of H_2-consumption is ~16 mmol/g. As shown in Figure 5, the H_2-TPR profile is composed of a (i) shoulder at lower temperature (ca. 200–260 °C) that could correspond to the reduction of some loosely bound Ni^{2+} based particles not engaged in the spinel in accordance with XPS experiments showing a slight excess of Ni (Fe:Ni = 1.9) and (ii) two neat reduction peaks with a maximum H_2-consumption at 341 and 543 °C which likely correspond to the reduction of most Ni^{2+} species to Ni° and Fe^{3+} to Fe°, respectively. These three steps were confirmed by TGA-DSC under H_2 which showed two main mass losses between 280 °C and 400 °C and between 400 °C and 600 °C, with a much larger loss for the second in good agreement with the reduction of nickel first followed by the reduction of iron at higher temperature (Figure 6). These two mass losses are preceded by two small mass losses, one before 100 °C likely due to traces of physisorbed water and the second between 200 and 300 °C, likely related to the reduction of nickel species at the catalyst surface. Assuming that all species of $NiFe_2O_4$ spinel structure are reduced, the theoretical mass loss of oxygen

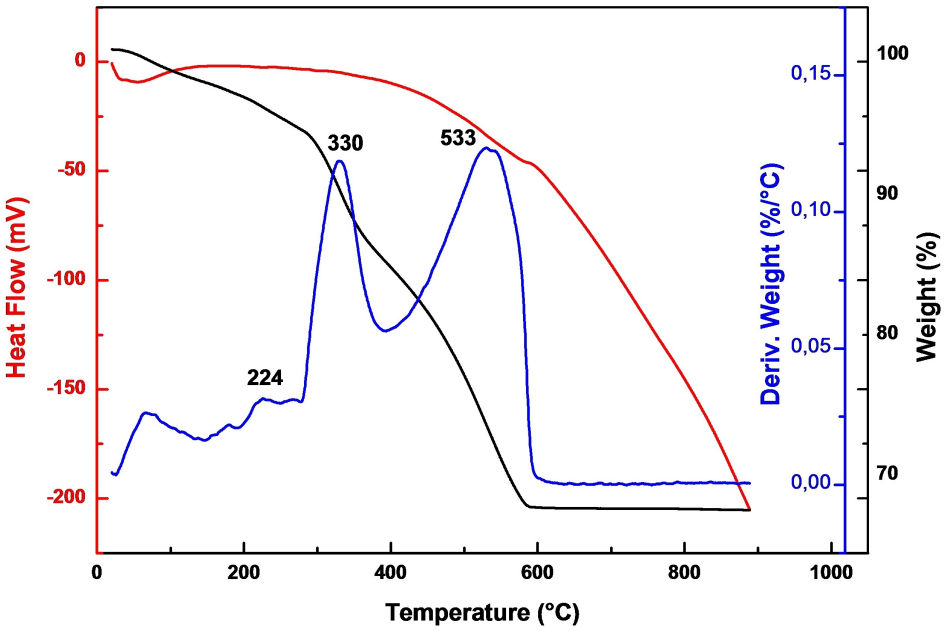

Figure 6. TGA-DSC thermograms of $NiFe_2O_4$ prepared via hydrothermal route at 180 °C/1 h

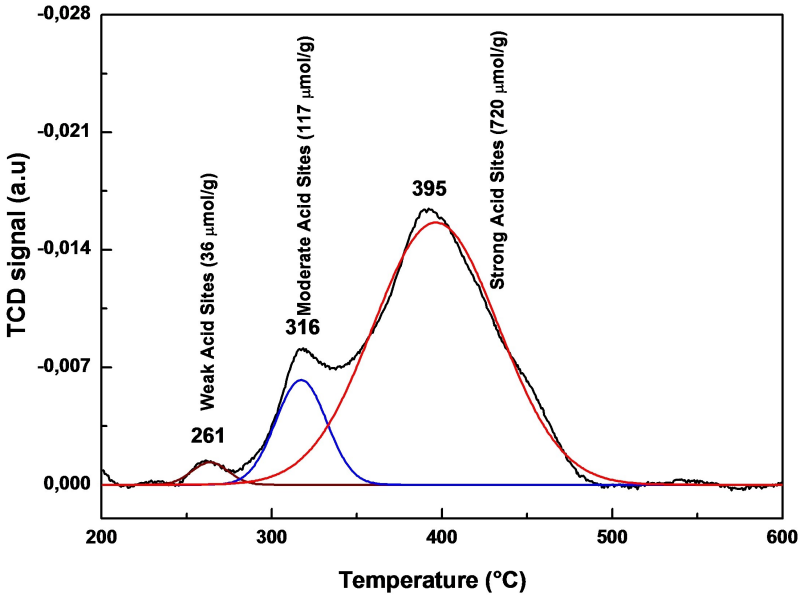

Figure 7. Ammonia TPD profile of $NiFe_2O_4$ prepared via hydrothermal route at 180 °C/1 h.

related to $NiFe_2O_4$ is 27.3 %. This value is close to value recorded from TGA curve under H_2 atmosphere (~30.6 %) with a difference of ~3.3 % which confirms a total reduction of Ni^{2+} and Fe^{3+} to metallic species in $NiFe_2O_4$ inverse spinel structure.

The reduction process of $NiFe_2O_4$ sample can be summarized as follows:

$$\text{Amb-} \sim 350\,^{\circ}\text{C}: \quad NiFe_2O_4 + H_2 \rightarrow Ni + Fe_2O_3 + H_2O \tag{1}$$

$$\sim 350\,^{\circ}\text{C} - 600\,^{\circ}\text{C}: \quad Fe_2O_3 + 3H_2 \rightarrow 2Fe + 3H_2O \tag{2}$$

during reduction by hydrogen (5 % H_2 in N_2) up to 1000 °C.

Acid properties (NH_3-TPD)

Figure 7 shows NH_3-TPD profile of $NiFe_2O_4$ sample. The desorption temperature indicates the acid strength of the sites, with weaker sites desorbing at lower temperature. After deconvolution of the NH_3-TPD curve, three regions could be distinguished for the

analyzed sample thus allowing to distinguish three types of acid sites: weak acid sites (~261 °C), moderate acid sites (316 °C) and strong acid sites (395 °C). The number of acid sites for each stage was calculated from the ammonia thermodesorption curves and the values are reported on Figure 7. The total number of acid sites corresponds to 873 μmol(NH_3)/g. It can be seen that the number of acid sites increased with the increase of temperature and the highest value (720 μmol(NH_3)/g) was observed at 395 °C. The low acid character observed at 261 °C can be linked to the presence of Ni^{2+} species on the surface which may act as basic character in accordance with XPS data at room temperature. The increase in the temperature induces certainly a change in surface composition and it seems that the acid character of the sample is favored at high temperature by the migration of Fe^{3+} species of the bulk, in particular those at octahedral sites, on the surface and increasing the number of acid sites because Fe^{3+} has an optical basicity greater than Ni^{2+} species (ΛFe^{3+} ($\Lambda tet = 0.659$) < Fe^{3+} ($\Lambda oct = 0.756$) < Ni^{2+} ($\Lambda oct = 0.953$).[25–27] Moreover, from these results, we can speculate about the absence of Brönsted sites, since it has been reported that Brönsted sites correspond to desorption temperatures higher than 400 °C,[28,29] which is not the case in our sample.

Catalytic data in isopropanol decomposition

The activity of $NiFe_2O_4$ catalyst was tested for isopropanol decomposition in the temperature range 200–400 °C without oxygen at atmospheric pressure. The catalyst shows no catalytic activity in isopropanol decomposition below 200 °C. The conversion of isopropanol and the selectivity to propylene and acetone, obtained on nickel ferrite oxide, are presented in Figures 8 and 9, respectively.

Propylene and acetone are the main products; propylene is due to the presence of acid sites, and acetone to that of basic/redox sites. The formation of isopropyl ether (condensation product) was not observed over our catalyst. The isopropanol conversion (Figure 8) increased with the reaction temperature. The evolution of acetone and propylene selectivity of the

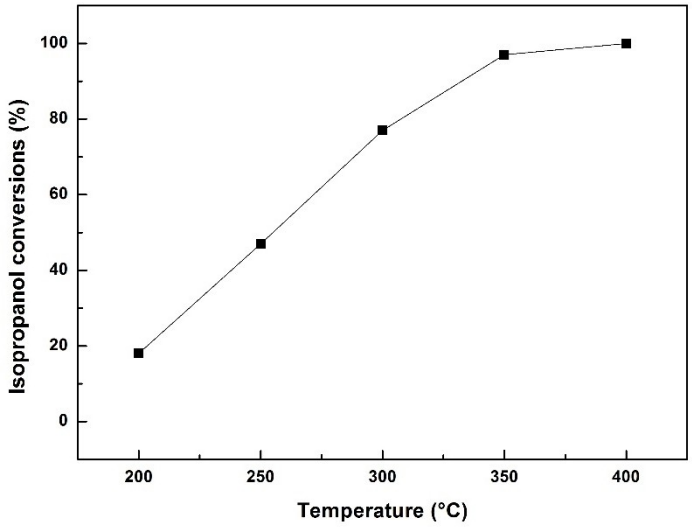

Figure 8. Isopropanol conversions of $NiFe_2O_4$ prepared via hydrothermal route at 180 °C/1 h.

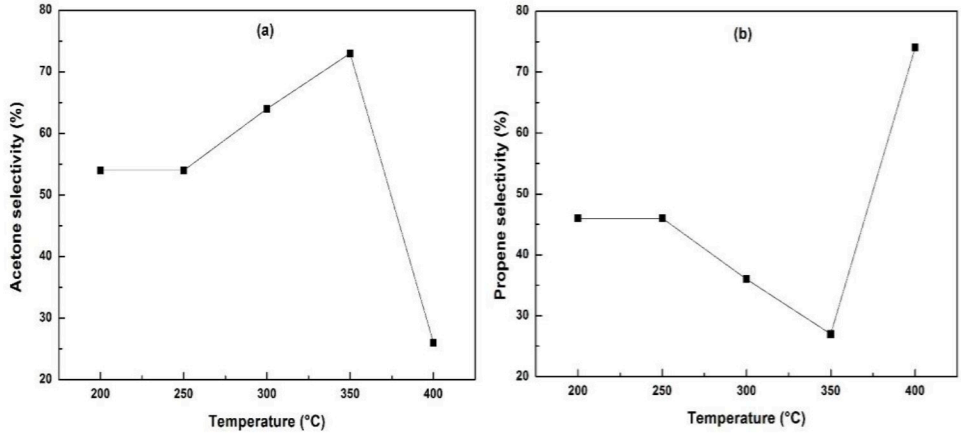

Figure 9. Acetone (a) and propylene (b) selectivity of $NiFe_2O_4$ prepared via hydrothermal route at 180 °C/1 h.

catalyst are depicted in Figure 9. The behavior of $NiFe_2O_4$ sample varies depending on the reaction temperature; acetone and propylene were observed throughout the temperatures range 200–400 °C, which means that both basic and acidic sites were available. At lower temperatures (200–350 °C), the formation of acetone is faster compared to that of propylene. However, when the reaction temperature increases from 350 to 400 °C, an opposite character was observed, the surface of $NiFe_2O_4$ catalyst becomes more acidic, indeed, the propylene selectivity increases at the expense of acetone by 27 to 74% between 350 and 400 °C (Figure 9). The proportion of acetone, with a maximum of 73% observed around 350 °C, undergoes a rapid drop to 400 °C (up to 26%).

The reaction rate R (μmol/h) calculated in the temperature range 200–350 °C is plotted in Figure 10. It is observed that the rate increases with increasing the reaction temperature up to 300 °C. Above this temperature, the rate mitigates dramatically and dropped up to 350 °C in accordance with acetone and propylene products distribution as observed above.

Correlation of the structural, textural and redox properties with catalytic decomposition

The observed behavior in catalytic activity is linked in our opinion to the textural properties and structural properties of the solid. The surface composition observed by XPS (Fe/Ni) is one of the main parameters responsible for surface properties such as acidity and basicity.

Isopropanol dehydrogenation and dehydration reactions to acetone and propylene, respectively, related to the contribution of both acidic and basic sites, is favored on our catalyst. In the light of properties determined by physicochemical characterizations, some considerations follow to tentatively account for these results.

It is worth noting that the structural and textural as well as redox properties affect significantly the catalytic activity of heterogeneous catalysts. In isopropanol decomposition reaction, little work can be found in the literature on the study of this model reaction. As already mentioned in the introduction, the decomposition occurs via two parallel elimination pathways: decomposition either leads to the formation of propylene and di-isopropyl either through dehydration on strong acidic sites (Brönsted and Lewis acid sites) or the formation of dehydrogenated product, acetone through the involvement of acid-base or redox sites.

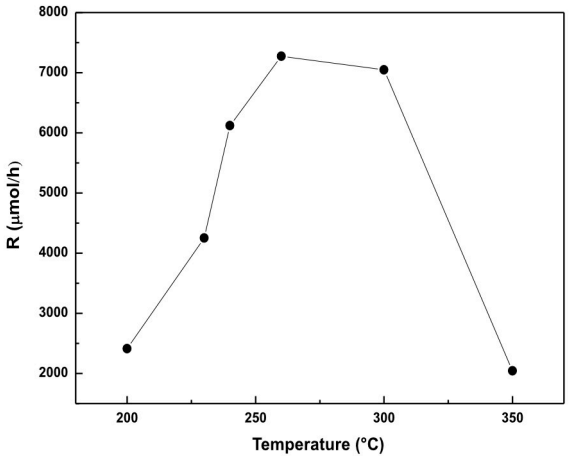

Figure 10. Variation of the reaction rate R (μmol/h) as function of the reaction temperature of $NiFe_2O_4$ prepared via hydrothermal route at 180 °C/1 h.

The catalytic activity in isopropanol decomposition reaction of $NiFe_2O_4$ catalyst show a dual character in the temperature range 200–400 °C suggesting that the role of the surface composition is responsible for the catalytic activity. The acidity of oxides can be compared using the optical basicity Λ, which allows comparison of the acidity of cations by taking into account their coordination and symmetry in the oxide.[25–27] The optical basicity Λ of inverse spinel $NiFe_2O_4$ is Λ = 0.771. For cations, it increases along the Fe^{3+} (Λtet = 0.659) < Fe^{3+} (Λoct = 0.756) < Ni^{2+} (Λoct = 0.953) series (tet and oct for tetrahedral and octahedral coordination, respectively). Both acidic and basic/redox sites were available during the temperature range studied was recorded in our spinel synthetized. In the temperature range 200–350 °C, a dehydrogenation pathway indicating the acetone formation was recorded and this behavior cover up when the reaction temperature increased up to 400 °C by propylene product formation. The binary character of $NiFe_2O_4$ sample is well correlated to their structural, textural and their redox properties. The formation of acetone in the temperature range 200–350 °C can be attributed to the localization of Ni^{2+} species on the surface of $NiFe_2O_4$ sample as showed by XPS and EDX experiments (Fe:Ni = 1.9). As mentioned previously the optical basicity Λ of Ni^{2+} cations are higher than those of Fe^{3+} species at octahedral or tetrahedral sites. In addition, the basic character of $NiFe_2O_4$ sample in the temperature range 200–350 °C can be well linked to the weak and moderate acid sites observed on this sample by NH_3-TPD experiments (Figure 7) at 261 °C (36 μmol(NH_3)/g) and 316 °C (117 μmol(NH_3)/g), respectively. The temperature range 350–400 °C is a turning point for $NiFe_2O_4$ spinel oxide prepared by hydrothermal synthesis, when the acid character appeared; this change is correlated certainly to the change in the surface composition and especially to the change in redox properties as observed by H_2-TPR and TGA-DSC analyses as well as to NH_3-TPD measurements. Indeed, the temperature range of character change to acidity through the formation of propylene of $NiFe_2O_4$ sample well coincides with the reduction temperature of Ni^{2+} and Fe^{3+} as affirmed by H_2-TPR and TGA-DSC analyses and also corroborate to the temperature of strong acid sites observed by NH_3-TDP- (Figure 7). The reducibility of a catalyst is a factor which greatly influences its catalytic activity towards redox reactions.[30,31] As affirmed previously by XRD analysis at higher temperatures under H_2 atmosphere,[32,33] $NiFe_2O_4$ is stable up to 300 °C and above this temperature Ni and Fe metallic were observed suggesting a change in redox properties from 300 °C leading to a change in acid-base behavior. The formation of propylene at 350–400 °C can be well explained to the high number of strong acid sites (720 μmol(NH_3)/g) at

395 °C as obtained by NH_3-TPD (Figure 7). Another suggestion to explain the dehydration pathway of our $NiFe_2O_4$ sample in 350–400 °C could be the migration, towards the surface, of Fe^{3+} species which is most acidic compared to Ni^{2+}[25–27,34] as confirmed by Raman technique, the presence of supplementary α-Fe_2O_3 oxidized phase in addition to the main $NiFe_2O_4$ spinel phase.

The decrease of the reaction rate in the temperature range 300–350 °C is probably due to two reasons: (i) first, to the drop of the specific surface area when the reaction temperature increased and (ii) the decrease of the surface basicity per unit mass (g) of catalyst as ascertained by NH_3-TPD.

Conclusions

Bulk ferrite spinel prepared using hydrothermal route with 114 m^2/g was investigated in isopropanol catalytic decomposition in the temperature range 200–400 °C. Structural properties evaluated by Raman spectroscopy shows, beside spinel structure, the presence of α-Fe_2O_3 as supplementary phase. The decomposition of isopropanol leads, on our catalyst, to the formation of propylene and acetone suggesting respectively the presence both acid sites and basic/redox sites on the surface of $NiFe_2O_4$ solid. The distribution of these products depends strongly to the distribution of Ni^{2+} and Fe^{3+} species on the surface; it changes depending on the reaction temperature. This evolution is probably linked to the evolution of the surface composition. Fe^{3+} would promote the formation of propylene, while nickel species would catalyze the formation of acetone. Our bulk $NiFe_2O_4$ issued from hydrothermal conditions having shown basic properties at low temperatures and acidic properties at high temperatures have probably undergone an evolution of the surface by migration of Fe^{3+} species from bulk to the surface.

Experimental

Catalysts Preparation

Nickel ferrite spinel was synthesized by hydrothermal method, using nitrates salts as precursors. NaOH (2 M) was added to an aqueous solution of $Ni(NO_3)_2 \cdot 6H_2O$ (0.05 M) and $Fe(NO_3)_3 \times 9H_2O$ (0.07 M) up to pH = 10 before loading in the hydrothermal cell. The cell was heated up to 180 °C for 1 hours. After reaction, the product was washed with distilled water and dried at 80 °C.

Characterization techniques

X-ray powder diffraction (XRD) was performed on a Bruker AXS D8 Advance diffractometer working in Bragg-Brentano geometry using Cu K_α radiation ($\lambda = 1.54$ Å), equipped with an energy dispersive detector (Sol-X). Patterns were collected at room temperature, in the $2\theta = 10$–$90°$ range, with a 0.02° step and 10 s counting time per step. The EVA software was used for phase identification. Laser Raman Spectroscopy (LRS) was performed using a Spectra Physics krypton ion laser at room temperature using the 647.1 nm excitation line. The beam was focused onto the samples using the macroscopic configuration of the apparatus. To avoid damage due to laser heating, all compounds were studied at a very low laser power (3 mW on the sample). Four accumulations were used in each spectral range. No damage of the material by the laser was observed. The scattered light was analysed with an XY Raman Dilor spectrometer equipped with an optical multichannel charge coupled device liquid nitrogen-cooled detector. The spectral resolution was 0.5 cm^{-1} in the 130–1500 cm^{-1} range. Acquisition and data processing were performed with the LABSPEC software. The specific surface area (S_{BET}) of the catalysts was determined by nitrogen adsorption at −196 °C with Micromeritics ASAP2010 apparatus. Scanning electron microscopy (SEM) and X-ray energy dispersive microanalysis (EDS) were carried out on HITACHI 4100S apparatus at 15 kV. Transmission electron microscopy (TEM) study was performed with a Philips CM200 and with a JEOL 2000EX. A suspension of the sample in ethanol was placed on a holey-carbon grid. X-ray photoelectron spectroscopy (XPS) at room temperature was carried out on Escalab 220 XL spectrometer (Vacuum Generators). A monochromatic Al K_α X-ray source was used and electron energies were measured in the constant analyzer energy mode. The pass energy was 100 eV for the survey of spectra and 40 eV for the single element spectra. All XPS binding energies were referred to C1s core level at 285 eV. The angle between the incident X-rays and the analyzer was 58°, photoelectrons being collected perpendicularly to the sample surface. Spectra were analyzed with the Casa-XPS software. The reducibility of the catalyst was also studied by temperature programmed reduction by hydrogen (H_2-TPR) and by thermal analysis TGA-DSC under H_2. H_2-TPR was carried out on Micromeritics-Autochem II 2920 with a TCD detector to monitor the H_2 consumption. After calibration of H_2 on the TCD, the sample displayed in a U-shaped quartz reactor was pre-treated in argon, and heated at 5 °C/min from 25 to 1000 °C in 5 % H_2 in Ar gas mixture. *In-situ* TGA-DSC under H_2 atmosphere was performed using a HidenIsochema gravimetric analyzer (model IGA-003) under 5 % H_2 in N_2 flow from 25 to 500 °C. Ca. 20 mg of sample was used. Measurements at 400 °C for 5 h under H_2 atmosphere were also carried out. The total acidity (Lewis + Brönsted) and acid strength distribution of catalysts were determined by temperature programmed desorption of ammonia (NH_3-TPD). The NH_3-TPD was performed using 150 mg of catalyst saturated with NH_3 (40 cm^3/min). After saturation, NH_3 weakly adsorbed was desorbed in a He flow, at the adsorption temperature, until no NH_3 was detected in the outlet gas. The NH_3-TPD was performed by raising the temperature up 550 °C at a heating rate of 5 °C/min. The NH_3 was measured by gas chromatography using a TCD detector.

Catalytic tests

The catalytic tests corresponding to isopropanol decomposition were carried out between 200 and 500 °C in a fixed bed continuous flow reactor under atmospheric pressure and in the absence of oxygen, by passing the carrier gas (Nitrogen) through a saturator containing the alcohol and maintained at 273 K. The weight of catalyst was ca. 0.05 g and the flow rate was 40 mL STP min^{-1}. Product analysis was performed by gas chromatography using a 10 % Carbowax 20 M on Chromosorb 200 column and a Flame Ionization Detector.

Acknowledgements

The Fonds Européen de Développement Régional (FEDER), CNRS, Région Hauts-de-France, Chevreul Institute (FR 2638) and Ministère de l'Education Nationale de l'Enseignement Supérieur et de la

Recherche are acknowledged for funding XPS/LEIS/ToF-SIMS spectrometers XRD and SEM instruments. The authors are also grateful to Olivier Gardol, Martine Trentesaux, Laurence Burylo and Nora Djelal for the technical assistance.

Conflict of Interest

All co-authors declare no conflict of interest.

Data Availability Statement

The data that support the findings of this study are available from the corresponding author upon reasonable request.

Keywords: acid-base properties · characterization · isopropanol · reducibility · spinel.

[1] H. G. Karge, V. Dondur, J. Weitkamp, *J. Phys. Chem.* **1991**, *95*, 283–288.
[2] A. Auroux, *Top. Catal.* **2002**, *19(3–4)*, 205–213.
[3] A. Auroux, *Top. Catal.* **1997**, *4(1–2)*, 71–89.
[4] S. Bennici, A. Auroux, J. Jackson D (eds), *Thermal Analysis and Calorimetric Methods*, Wiley-VCH Verlag GmbH & Co. KGaA, **2009**, pp. 391–441.
[5] L. M. Kustov, *Top. Catal.* **1997**, *4(1–2)*, 131–144.
[6] M. Stocker, *Microporous Mater.* **1996**, *6(5–6)*, 235–237.
[7] S. A. Bocanegra, A. D. Ballarini, O. A. Scelza, S. R. De Miguel, *Mater. Chem. Phys.* **2008**, *111(2–3)*, 534–544.
[8] J. A. Wang, X. Bokhimi, O. Novaro, T. Lopez, R. Gomez, *J. Mol. Catal. A* **1999**, *145(1–2)*, 291–300.
[9] C. Ancion, G. Poncelet, *Appl. Catal. A* **1994**, *108*, 31–40.
[10] J. C. Luy, J. M. Parera, *Appl. Catal.* **1984**, *13(1)*, 39–48.
[11] R. Grabowski, B. Grzybowska, K. Samson, J. Słoczyński, J. Stoch, K. Wcisło, *Applied Catalysis A. Gen.* **1995**, *125(1)*, 129–144.
[12] M. A. Aramendia, V. Borau, C. Jimenez, J. M. Marinas, A. Porras, F. G. Urbano, *J. Catal.* **1996**, *161*, 829–838.
[13] A. Gervasini, A. Auroux, *J. Catal.* **1991**, *131(1)*, 190–198.
[14] A. Gervasini, A. Auroux, *J. Phys. Chem.* **1990**, *94(16)*, 6371–1379.
[15] P. N. Trikalitis, P. J. Pomonis, *Appl. Catal. A* **1995**, *131(2)*, 309–322.
[16] R. Benrabaa, A. Löfberg, J. Guerrero Caballero, E. Bordes-Richard, A. Rubbens, R. N. Vannier, H. Boukhlouf, A. Barama, *Catal. Commun.* **2015**, *58*, 127–131.
[17] K. N. Subramanyam, *J. Phys. C.* **1971**, *4*, 2266.
[18] M. N. Iliev, D. Mazumdar, J. X. Ma, A. Gupta, F. Rigoto, J. Fonctcuberta, *Phys. Rev.* **2011**, *B83*, 014108.
[19] A. Ahlawat, V. G. Sathe, V. R. Reddy, A. Gupta, *J. Magn. Magn. Mater.* **2011**, *323(15)*, 2049–2054.
[20] D. Varshney, K. Verma, *Mater. Chem. Phys.* **2013**, *140*, 412–418.
[21] L. C. Prinsloo, P. Colomban, J. D. Brink, I. Meiklejohn, *J. Raman Spectrosc.* **2011**, *42(4)*, 626–632.
[22] M. Giarola, G. Mariotto, D. Ajo, *J. Raman Spectrosc.* **2012**, *43(4)*, 556–558.
[23] http://www.xpsfitting.com.
[24] V. K. Mittal, S. Bera, R. Nithya, M. P. Srinivasan, S. Velmurugan, S. V. Narasimhan, *J. Nucl. Mater.* **2004**, *335(3)*, 302–310.
[25] P. Moriceau, A. Lebouteiller, E. Bordes, P. Courtine, *Phys. Chem. Chem. Phys.* **1999**, *1(24)*, 5735–5744.
[26] E. Bordes-Richard, *Top. Catal.* **2008**, *50(1-4)*, 82–89.
[27] E. Bordes-Richard, P. Courtine, *Optical Basicity: a Scale of Acidity/Basicity of Solids and its Application to Oxidation Catalysis*, in: J. L. J. Fierro (Ed.), Metal Oxides: Chemistry and Applications, Marcel Dekker, **2005**.
[28] D. Das, H. K. Mishra, A. K. Dalai, K. M. Parida, *Appl. Catal. A.* **2003**, *243(2)*, 271–284.
[29] H. Zou, Y. S. Lin, *Appl. Catal. A Gener.* **2004**, *265(1)*, 35–42.
[30] W. Shan, W. Shen, C. Li, *Chem. Mater.* **2003**, *15(25)*, 4761–4767.
[31] B. M. Mogudi, P. Ncube, R. Meijboom, *Applied Catalysis B: Environm.* **2016**, *198*, 74–82.
[32] R. Benrabaa, H. Boukhlouf, A. Löfberg, A. Rubbens, R. N. Vannier, E. Bordes-Richard, A. Barama, *J. Nat. Gas Chem.* **2012**, *21(5)*, 595–604.
[33] R. Benrabaa, A. Löfberg, A. Rubbens, E. Bordes-Richard, R. N. Vannier, A. Barama, *Catal. Today* **2013**, *203*, 188–195.
[34] C. G. Ramankutty, S. Sugunan, B. Thomas, *J. Mol. Catal. A* **2002**, *187(1)*, 105–117.

Submitted: November 10, 2022
Accepted: January 12, 2023